ATLAS Note

GROUP-2017-XX

24th September 2020

Draft version 0.1

1

EFT Interpretations of $t\bar{t}H$ Production in Multilepton Final States at $\sqrt{s}$ = 13 TeV

The ATLAS Collaboration

The possibility of using the kinematic properties of the Higgs boson to search for new physics is investigated using $t\bar{t}H$ events with multiple leptons in the final state. A deep neural-network is used to reconstruct the momentum spectrum of the Higgs, which would be altered by the presence of new physics without affecting the overall rate of $t\bar{t}H$ production. Simulations representing 139 fb^{-1} at $\sqrt{s}$ = 13 TeV are used to place expected limits on physics 'beyond the Standard Model' affecting the coupling of the Higgs boson to the top quark.

Contents

1 Changes and outstanding items

1.1 Changelog

This is version 1

2 Introduction

Since the discovery of a Higgs boson compatable with the Standard Model (SM) in 2012 [], its interactions with other particles have been studied using proton-proton collision data produced by the Large Hadron Collider (LHC). The strongest of these interactions is the coupling of the Higgs to the top quark, making the Yukawa coupling between these two particles of particular interest for study.

These interactions can be measured directly by studying the production of a Higgs Boson in association with a pair of Top Quarks ($t\bar{t}H$) []. While this process has been observed by both the ATLAS [] and CMS [] collaborations, these analyses have focused on measuring the overall rate of $t\bar{t}H$ production. There are several theories of physics Beyond the Standard Model (BSM), however, that would affect the kinematics of $t\bar{t}H$ production without altering its overall rate [].

An Effective Field Theory approach can be used to model the low energy effects of new, high energy physics, by paramaterizing BSM effects as dimension-six operators. The addition of these operators can be shown to modify the transverse momentum (p_T) spectrum of the Higgs Boson []. Therefore, reconstructing the momentum spectrum of the Higgs provides a means to observe new physics in the Higgs sector.

This note reports on the feasability of measuring the impact of dimension-six operators in $t\bar{t}H$ events with multiple leptons in the final state, using Monte Carlo (MC) simulations scaled to 139 fb^{-1} at an energy $\sqrt{s} = 13$ TeV. Events are separated into channels based on the number of light leptons (electrons and muons) in the final state - either two same-sign leptons (2lSS), or three leptons (3l). A deep neural network is used to identify which objects originate from the decay of the Higgs, and reconstruct the momentum of the Higgs Boson in each event. This reconstructed momentum spectrum is used to place limits on BSM effects, and on the parameters of dimension-six operators.

This note is organized as follows: Section **??** describes the LHC and the ATLAS detector. The dataset and Monte Carlo (MC) simulations used in the analysis is outlined in section **??**. Section **??** describes the identification and reconstruction of the various physics objects. The models used to reconstruct the momentum spectrum of the Higgs is discussed in section **??**. The selection and categorisation of events comprises section **??**, and the theoritical and experimental systematic uncertainties considered are described in section **??**. Finally, the results of the study are summarized in section **??**.

3 The ATLAS Detector

ATLAS is a general purpose detector designed to maximize the detection efficiency of nearly all physics objects, including leptons, jets, and photons, while covering nearly the entire solid angle around the collision point. Just surrounding the interaction point is the Inner Detector, designed

to track the path of charged particles moving through the detector. An inner solenoid surrounding the Innder Detector is used to produces a magnetic field of 2 T.

The Inner Detector consists of three components - the Pixel Detector, the Semi-Conductor Tracker (SCT), and the Transition Radiation Tracker (TRT). The Pixel Detector is the innermost of these, beginning just 33.25 mm away from the beam line. It consists of three silicon layers along the barrel, as well as three endcap layers, covering a range of $|\eta| < 2.5$. The Semiconductor Tracker (SCT) is similar to the Pixel detector, but uses long strips rather than small pixel to cover a larger spatial area.

Situated outside the Innder Detector are two concentric calorimeters, covering a range of $|\eta|<4.9$. The inner calorimeter uses liquid argon (LAr) to measure energy of particles that interact electromagnetically within the region $|\eta| < 3.2$, and consists of around 180,000 readout channels. The outer calorimeter, or hadronic calorimeter, is composed of steel plates, with scintillating tiles as the active material. It covers a range of $|\eta| < 1.7$, and the signals from the hadronic calorimeter are read out by photomultiplier tubes (PMTs). The remain pseudorapidity range is covered by forward calorimeter modules.

The outermost layer of the detector, the muon spectrometer, consists of tracking and triggering system. It extends from the outside of the calormeter system, about a 4.25 m radius from the beam line, to a radius of 11 m. Two large toroidal magnets within the muon system generate a large magnetic ranging between 2 T and 8 T. 1200 tracking chambers are placed in the muon system in order to precisely measure the tracks of muons within $|\eta| < 2.7$ with high spatial resolution.

A two-level trigger system is used to select out events to be recorded. The level-1 trigger uses hardware information from the calorimeters and muon spectrometer to select events that contain candidates for particles commonly used in analysis, and reduces the rate of events from 40 MHz to around 100 kHz. Events that pass the level-1 trigger move to the High-Level Trigger (HLT). The HLT takes place outside of the detector in software, and looks for properties such as a large amount of missing transverse energy, well defined leptons, and multiple high energy jets. Events that pass the HLT are stored and used for analysis. Because the specifics of the HLT are determined by software rather than hardware, the thresholds can be changed throughout the run of the detector in response to run conditions such as changes to pilup and luminosity. After the HLT is applied, the event rate is reduced to around 1 kHz, which are recorded for analysis.

4 Data and Monte Carlo Samples

For both data and Monte Carlo (MC) simulations, samples were prepared in the `xAOD` format, which was used to produced a `xAOD` based on the `HIGG8D1` derivation framework. This framework was designed for the main $t\bar{t}H$ multi-lepton analysis. Because this analysis targets events with multiple light leptons, as well as tau hadrons, this framework skims the dataset of any events that do not meet at least one of the following requirements:

- at least two light leptons within a range |η|<2.6, with leading lepton p_T > 15 GeV and subleading lepton p_T > 5 GeV

- at least one light lepton with p_T > 15 GeV within a range |η|<2.6, and at least two hadronic taus with p_T > 15 GeV.

Samples were then generated from these `HIGG8D1` derivations using a modified version of AnalysisBase version 21.2.127.

4.1 Data Samples

The study uses proton-proton collision data collected by the ATLAS detector from 2015 through 2018, which represents an integrated luminosity of 139 fb^{-1} and an energy of $\sqrt{s} = 13$ TeV. All data used in this analysis was included in one the following Good Run Lists:

- data15_13TeV.periodAllYear_DetStatus-v79-repro20-02_DQDefects-00-02-02 _PHYS_StandardGRL_All_Good_25ns.xml

- data16_13TeV.periodAllYear_DetStatus-v88-pro20-21_DQDefects-00-02-04 _PHYS_StandardGRL_All_Good_25ns.xml

- data17_13TeV.periodAllYear_DetStatus-v97-pro21-13_Unknown_PHYS_StandardGRL _All_Good_25ns_Triggerno17e33prim.xml

- data18_13TeV.periodAllYear_DetStatus-v102-pro22-04_Unknown_PHYS_StandardGRL _All_Good_25ns_Triggerno17e33prim.xml

4.2 Monte Carlo Samples

Several Monte Carlo (MC) generators were used to simulate both signal and background processes. For all of these, the effects of the ATLAS detector are simulated in Geant4. The specific event generator used for each of these MC samples is listed in table **??**.

Table 1: The configurations used for event generation of signal and background processes, including the event generator, matrix element (ME) order, parton shower algorithm, and parton distribution functin (PDF).

Process	Event generator	ME order	Parton Shower	PDF
$t\bar{t}H$	MG5_aMC	NLO	Pythia 8	NNPDF 3.0 NLO [**Ball:2014uwa**]
	(MG5_aMC)	(NLO)	(Herwig++)	(CT10 [**ct10**])
$t\bar{t}W$	MG5_aMC	NLO	Pythia 8	NNPDF 3.0 NLO
	(Sherpa 2.1.1)	(LO multileg)	(Sherpa)	(NNPDF 3.0 NLO)
$t\bar{t}(Z/\gamma^* \to ll)$	MG5_aMC	NLO	Pythia 8	NNPDF 3.0 NLO
VV	Sherpa 2.2.2	MEPS NLO	Sherpa	CT10
$t\bar{t}$	Powheg-BOX v2 [**powhegtt**]	NLO	Pythia 8	NNPDF 3.0 NLO
$t\bar{t}\gamma$	MG5_aMC	LO	Pythia 8	NNPDF 2.3 LO
tZ	MG5_aMC	LO	Pythia 6	CTEQ6L1
$tHqb$	MG5_aMC	LO	Pythia 8	CT10
tHW	MG5_aMC	NLO	Herwig++	CT10
	(Sherpa 2.1.1)	(LO multileg)	(Sherpa)	(NNPDF 3.0 NLO)
tWZ	MG5_aMC	NLO	Pythia 8	NNPDF 2.3 LO
$t\bar{t}t$, $t\bar{t}t\bar{t}$	MG5_aMC	LO	Pythia 8	NNPDF 2.3 LO
$t\bar{t}W^+W^-$	MG5_aMC	LO	Pythia 8	NNPDF 2.3 LO
s-, t-channel, Wt single top	Powheg-BOX v1 [**powhegstp**]	NLO	Pythia 6	CT10
$qqVV$, VVV				
$Z \to l^+l^-$	Sherpa 2.2.1	MEPS NLO	Sherpa	NNPDF 3.0 NLO

5 Object Reconstruction

All analysis channels considered in this note share a common object selection for leptons and jets, as well as a shared trigger selection.

5.1 Trigger Requirements

Events are required to be selected by dilepton triggers, as summarized in table **??**.

5.2 Light Leptons

Electron candidates are reconstructed from energy clusters in the electromagnetic calorimeter that are associated with charged particle tracks reconstructed in the inner detector [**ATLAS-CONF-2016-024**]. Electron candidates are required to have $p_T > 10$ GeV and $|\eta_{cluster}| < 2.47$. Candidates in the transition region between different electromagnetic calorimeter components, $1.37 < |\eta_{cluster}| < 1.52$, are rejected. A multivariate likelihood discriminant combining shower shape and track information is used to distinguish prompt electrons from nonprompt leptons, such as those originating from hadronic showers.

Dilepton triggers (2015)	
$\mu\mu$ (asymm.)	`HLT_mu18_mu8noL1`
ee (symm.)	`HLT_2e12_lhloose_L12EM10VH`
$e\mu$, μe ($\sim$symm.)	`HLT_e17_lhloose_mu14`
Dilepton triggers (2016)	
$\mu\mu$ (asymm.)	`HLT_mu22_mu8noL1`
ee (symm.)	`HLT_2e17_lhvloose_nod0`
$e\mu$, μe ($\sim$symm.)	`HLT_e17_lhloose_nod0_mu14`
Dilepton triggers (2017)	
$\mu\mu$ (asymm.)	`HLT_mu22_mu8noL1`
ee (symm.)	`HLT_2e24_lhvloose_nod0`
$e\mu$, μe ($\sim$symm.)	`HLT_e17_lhloose_nod0_mu14`
Dilepton triggers (2018)	
$\mu\mu$ (asymm.)	`HLT_mu22_mu8noL1`
ee (symm.)	`HLT_2e24_lhvloose_nod0`
$e\mu$, μe ($\sim$symm.)	`HLT_e17_lhloose_nod0_mu14`

Table 2: List of lowest p_T-threshold, un-prescaled dilepton triggers used for 2015-2018 data taking.

To further reduce the non-prompt contribution, the track of each electron is required to originate from the primary vertex; requirements are imposed on the transverse impact parameter significance ($|d_0|/\sigma_{d_0}$) and the longitudinal impact parameter ($|\Delta z_0 \sin\theta_\ell|$), as shown in table **??**.

Muon candidates are reconstructed by combining inner detector tracks with track segments or full tracks in the muon spectrometer [**PERF-2014-05**]. Muon candidates are required to have $p_T > 10$ GeV and $|\eta| < 2.5$. All leptons are required to be isolated, and pass a non-prompt BDT selection described in detail in [**ttH_paper**].

5.3 Jets

Jets are reconstructed from calibrated topological clusters built from energy deposits in the calorimeters [**ATL-PHYS-PUB-2015-015**], using the anti-k_t algorithm with a radius parameter $R = 0.4$. Jets with energy contributions likely arising from noise or detector effects are removed from consideration [**ATLAS-CONF-2015-029**], and only jets satisfying $p_T > 25$ GeV and $|\eta| < 2.5$ are used in this analysis. For jets with $p_T < 60$ GeV and $|\eta| < 2.4$, a jet-track association algorithm is used to confirm that the jet originates from the selected primary vertex, in order to reject jets arising from pileup collisions [**PERF-2014-03**].

5.4 Missing Transverse Energy

Because all $t\bar{t}H - ML$ channels considered include multiple neutrinos, missing transverse energy (E_T^{miss}) is present in each event. The missing transverse momentum vector is defined as the inverse of the sum of the transverse momenta of all reconstructed physics objects as well as remaining unclustered energy, the latter of which is estimated from low-p_T tracks associated with the primary vertex but not assigned to a hard object [**ATL-PHYS-PUB-2015-027**].

6 Higgs Momentum Reconstruction

Reconstructing the momentum of the Higgs boson is a particular challenge for channels with leptons in the final state: Because all channels include at least two neutrinos in the final state, the Higgs can never be fully reconstructed. However, the momentum spectrum can be well predicted by a neural network when provided with the four-vectors of the Higgs Boson decay products, as shown in section **??**. With this in mind, a sophisticated approach involving several layers of MVAs is used to reconstruction the Higgs momentum.

The first layer is a Neural Network designed to select which jets are most likely to be the b-jets that came from the top decay. The kinematics of these jets are fed into the second layer, also a BDT, which is designed to identify the decay products of the Higgs Boson itself. The kinematics of these particles are then fed into a deep neural-network, which predicts the momentum of the Higgs.

6.1 Truth Level Reconstruction

Machine Learning algorithms are trained to identify the decay products of the Higgs Boson using MC simulations of $t\bar{t}H$ events. Reconstructed physics objects are matched to truth level particles, in order to identify the parents of these reconstructed objects.

6.2 b-jet Identification

Including the kinematics of the b-jets that originate from the top decay is found to improve the identification of the Higgs decay products, and improve the accuracey with which the Higgs momentum can be reconstructed. Because these b-jets are reconstructed by the detector with high efficiency (just over 90% of the time), and can be identified relatively consistently, the first step in reconstructing the Higgs is selecting the b-jets from the top decay.

Exactly two b-jets are expected in the final state of $t\bar{t}H - ML$ events. However, in both the 3l and 2lSS channels, only one or more b-tagged jets are required (where the 70% DL1r b-tag working point is used). Therefore, for events which have exactly one, or more than two, b-tagged jets, deciding which combination of jets correspond to the top decay is non-trivial. Further, events

with 1 b-tagged jet represent just over half of all $t\bar{t}H - ML$ events. Of those, both b-jets are reconstructed by the detector 70% of the time. Therefore, rather than adjusting the selection to require exactly 2 b-tagged jets, and losing more than half of the signal events, a neural network is used to predict which pair of jets is most likely to correspond to truth b-jets.

The kinematics of each possible pairing of jets are used to train the network, where the pairing that includes both truth b-jets is assigned a label of 1, and all other pairings a label of 0. Further details concerning the models, including the specific input variables, hyperparameters, and performance metrics, can be found in **??**

For each event, all pairings of jets are fed into the model, and the pair of jets with the highest output score are taken to be b-jets in successive steps of the analysis. This procedure is found to identify the correct pairing of jets for 73% of 2lSS signal events, and 78% of 3l signal events.

6.3 Higgs Reconstruction

Techniques similar to the b-jet identification algorithms are employed to select the decay products of the Higgs.

6.4 p_T Prediction

Once the most probable decay products have been identified, their kinematics are used to reconstruct the momentum spectrum of the Higgs Boson.

6.5 3l Decay Mode

In the 3l channel, there are two possible ways for the Higgs to decay, both involving intermediate W boson pairs: Either both W bosons decay leptonically, in which case the reconstructed decay consists of two leptons (referred as the fully-leptonic 3l channel), or one W decays leptonically and the other hadronically, giving two jets and one lepton in the final state (referred to as the semi-leptonic 3l channel). In order to accurately reconstruct the Higgs, it is necessary to identify which of these decays took place for each 3l event.

7 Signal Region Definitions

Events are divided into two channels based on the number of leptons in the final state: one with two same-sign leptons, the other with three leptons. The 3l channel includes events where both leptons originated from the Higgs boson as well as events where only one of the leptons

7.1 Pre-MVA Event Selection

A preselection is applied to define orthogonal analysis channels based on the number of leptons in each event.

7.1.1 2lSS Channel

7.1.2 3l Channel

7.2 Event MVA

Separate multi-variate analysis techniques (MVAs) are used in order to distinguish signal events from background for each analysis channel - 2lSS, 3l semi-leptonic, and 3l fully leptonic. In particular, Neural Networks produced with Tensorflow are trained using the kinematics of signal and background events derived from Monte Carlo simulations. Further, because the background composition differs for events with a high reconstructed Higgs p_T compared to events with low reconstructed Higgs p_T, separate MVAs are produced for high and low p_T regions.

7.2.1 2lSS - High p_T

7.2.2 2lSS - Low p_T

7.2.3 3l Semi-Leptonic - High p_T

7.2.4 3l Semi-Leptonic - Low p_T

7.2.5 3l Fully Leptonic - High p_T

7.2.6 3l Fully Leptonic - Low p_T

7.3 Signal Region Definitions

Once pre-selection has been applied, channels are further refined based on the MVAs described above. The output of the model described in section **??** is used to separate the three channel into two - Semi-leptonic and Fully-leptonic - based on the predicted decay mode of the Higgs boson.

For each event, depending on the channel as well as the predicted p_T of the Higgs derived from the algorithm described in section **??**, a cut on the appropriate background rejection algorithm is applied. The specific selection used, and the event yield in each channel after this selection has been applied, is summarized below.

225 **7.3.1** 2lSS

226 **7.3.2** 3l − Semi − leptonic

227 **7.3.3** 3l − Fully − leptonic

228 # 8 Systematic Uncertainties

229 The systematic uncertainties that are considered are summarized in table **??**. These are imple-
230 mented in the fit either as a normalization factors or as a shape variation or both in the signal
231 and background estimations. The numerical impact of each of these uncertainties is outlined in
232 section **??**.

Table 3: Sources of systematic uncertainty considered in the analysis. Some of the systematic uncertainties are split into several components, as indicated by the number in the rightmost column.

Systematic uncertainty	Components
Luminosity	1
Pileup reweighting	1
Physics Objects	
Electron	6
Muon	15
Jet energy scale and resolution	28
Jet vertex fraction	1
Jet flavor tagging	131
E_T^{miss}	3
Total (Experimental)	186
Background Modeling	
Cross section	24
Renormalization and factorization scales	10
Parton shower and hadronization model	2
Shower tune	4
Total (Signal and background modeling)	40
Background Modeling	
Cross section	24
Renormalization and factorization scales	10
Parton shower and hadronization model	2
Shower tune	4
Total (Signal and background modeling)	40
Total (Overall)	226

The uncertainty in the combined 2015+2016 integrated luminosity is derived from a calibration of the luminosity scale using x-y beam-separation scans performed in August 2015 and May 2016 [**lumi**].

The experimental uncertainties are related to the reconstruction and identification of light leptons and and b-tagging of jets, and to the reconstruction of E_T^{miss}. The sources which contribute to the uncertainty in the jet energy scale [**jes**] are decomposed into uncorrelated components and treated as independent sources in the analysis.

The uncertainties in the b-tagging efficiencies measured in dedicated calibration analyses [**btag_cal**] are also decomposed into uncorrelated components. The large number of components for b-tagging is due to the calibration of the distribution of the BDT discriminant.

The systematic uncertainties associated with the signal and background processes are accounted for by varying the cross-section of each process within its uncertainty.

9 Results

A maximum likelihood fit is performed simultaneously over the regions described in section **??**.

10 Conclusion

As search for the effects of dimension-six operators on $t\bar{t}H$ production is performed. An effective field theory approached is used to parameratize the effects of high energy physics on the Higgs momentum spectrum. The momentum spectrum is reconstructed using various MVA techniques, and the limits on dimension-six operators are limited to X.

List of contributions

Appendices

A Machine Learning Models

The following section provides details regarding the various machine learning models used in the analysis. The Keras neural network framework, with Tensorflow as the backend, is used to create each model, and the number of hidden layers and nodes are determined using grid search optimization. For each model, a LeakyReLU activation function is used, along with a learning rate of 0.01, and the Adam optimization algorithm. For the classification algorithms (b-jet matching, Higgs reconstruction, and background separation) binary-cross entropy is used as the loss function.

A.1 Higgs Reconstruction Algorithms

A.1.1 b-jet MVA - 2lSS Channel

For the 2lSS channel, the following input features as used for training:

$M(j_0 j_1)$	$M(j_0 j_1 l_0 l_1 E_T^{miss})$	$M(l_0 j_0)$
$M(l_0 j_1)$	$M(l_1 j_0)$	$M(l_1 j_1)$
$p_T(j_0 j_1 l_0 l_1 E_T^{miss})$	$\Delta\phi(j_0)(E_T^{miss})$	$\Delta\phi(j_1)(E_T^{miss})$
$\Delta R(j_0)(j_1)$	$\Delta R(j_0 l_0)(j_1 l_1)$	$\Delta R(j_0 l_1)(j_1 l_0)$
$\Delta R(l_0)(j_0)$	$\Delta R(l_0)(j_1)$	$\Delta R(l_1)(j_0)$
$\Delta R(l_1)(j_1)$	jet DL1r 0	jet DL1r 1
jet η 0	jet η 1	jet p_T 0
jet p_T 1	jet rankDL1r 0	jet rankDL1r 1
Lepton p_T 0	Lepton p_T 1	E_T^{miss}
nJets	nJets OR DL1r 60	nJets OR DL1r 85

Table 4: Input features used in the 2lSS b-jet identification algorithm

Based on the results of grid search evaluation, the optimal architecture is found to include 5 hidden layers with 40 nodes each. A learning rate of 0.01 is used, and leakyReLU is used as an activation function. The output score distribution as well as the ROC curve for the trained model are shown in figure **??**.

A.1.2 b-jet MVA - 3l Channel

Based on the results of grid search evaluation, the optimal architecture is found to include 5 hidden layers with 40 nodes each. The output score distribution as well as the ROC curve for the trained model are shown in figure **??**.
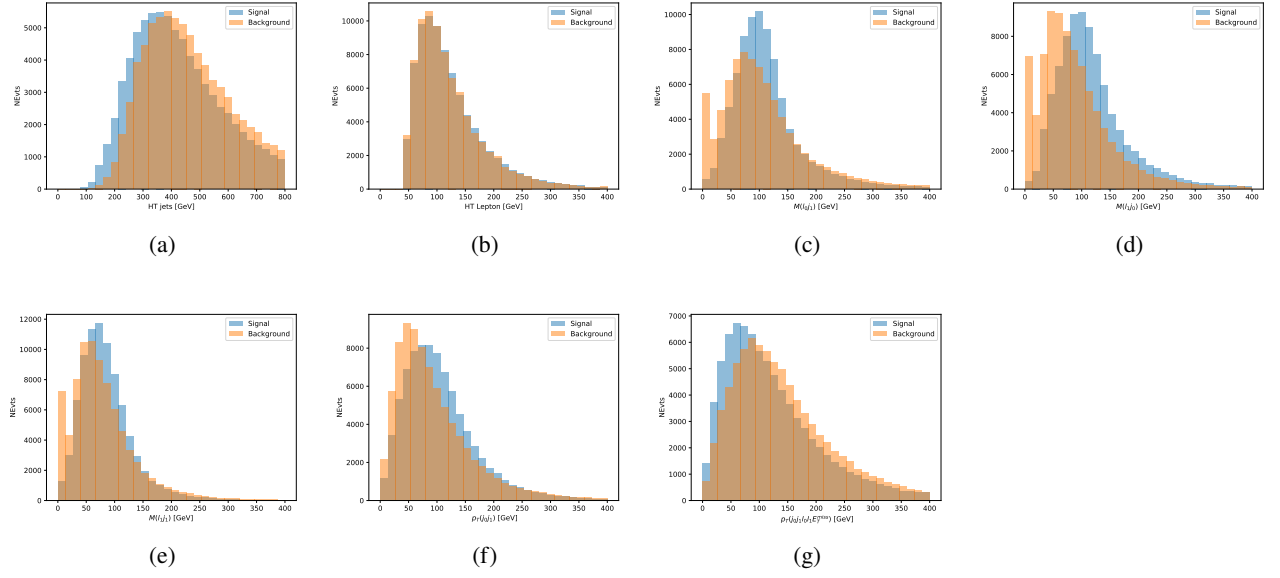
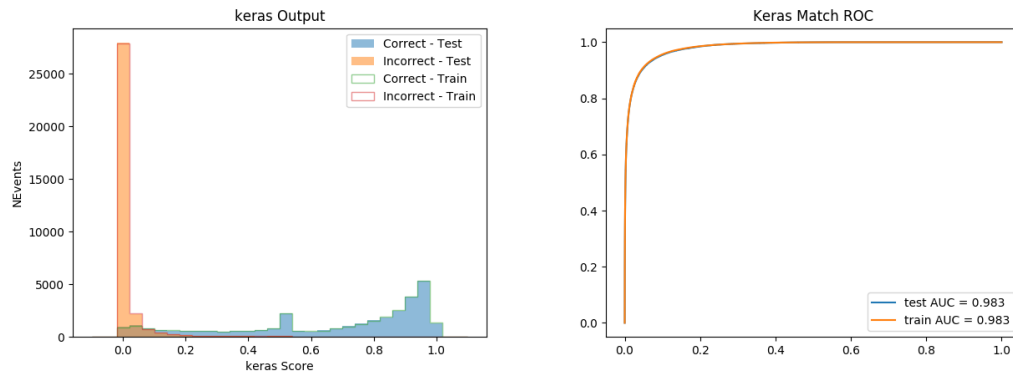Figure A.1: Input features for top2lSS training

Figure A.2: (left) the output score of the NN for correct and incorrect combinations of jets. (right) the ROC curve...
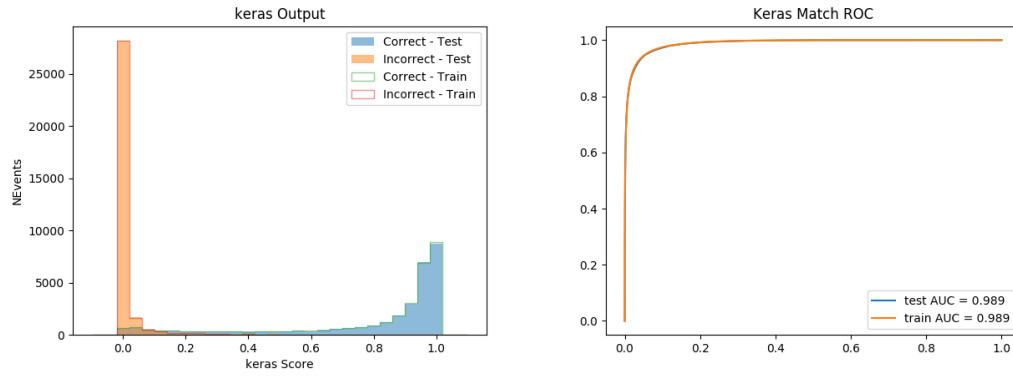
Figure A.3: tmp

A.1.3 Higgs Reconstruction MVA - 2lSS Channel

A.1.4 Higgs Reconstruction MVA - 3l Semi-leptonic Channel

A.1.5 Higgs Reconstruction MVA - 3l Fully-leptonic Channel

A.2 p_T Prediction MVA

A.3 2lSS Channel

A.4 3l Semi-leptonic Channel

A.5 3l Fully-leptonic Channel

A.6 3l Decay MVA

Separate multi-variate analysis techniques (MVAs) are used in order to distinguish signal events from background for each analysis channel - 2lSS, 3l semi-leptonic, and 3l fully leptonic. In particular, Neural Networks produced with Tensorflow are trained using the kinematics of signal and background events derived from Monte Carlo simulations. Further, because the background composition differs for events with a high reconstructed Higgs p_T compared to events with low reconstructed Higgs p_T, separate MVAs are produced for high and low p_T regions.
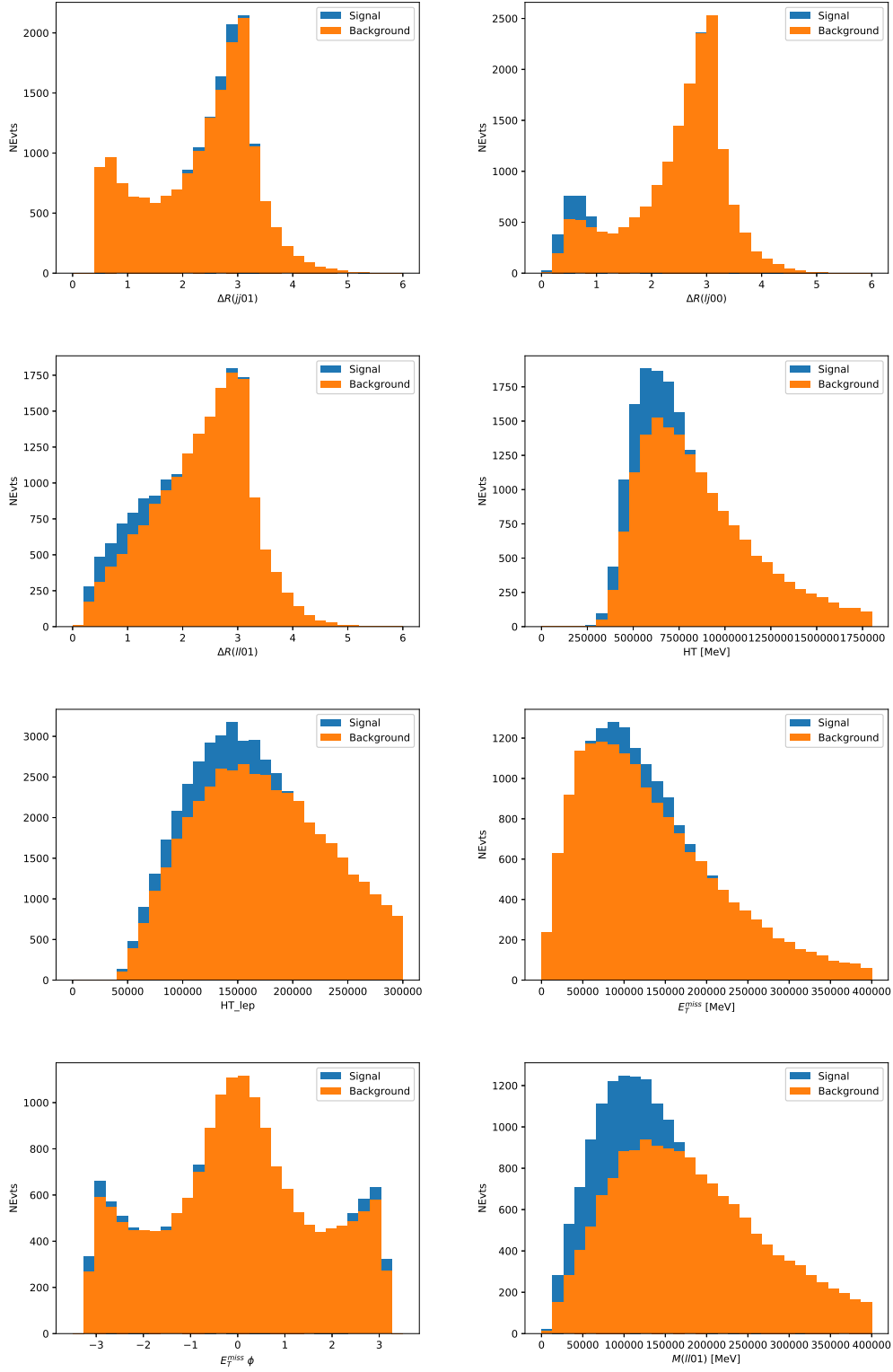
Figure A.4:

A.7 2lSS

A.7.1 2lSS - High p_T

A.7.2 2lSS - Low p_T

A.8 3l Semi-Leptonic

A.8.1 3l Semi-Leptonic - High p_T

A.8.2 3l Semi-Leptonic - Low p_T

A.9 3l Fully Leptonic

A.9.1 3l Fully Leptonic - High p_T

A.9.2 3l Fully Leptonic - Low p_T